Excited Excitonic States in 1L, 2L, 3L, and Bulk WSe$_2$ Observed by Resonant Raman Spectroscopy
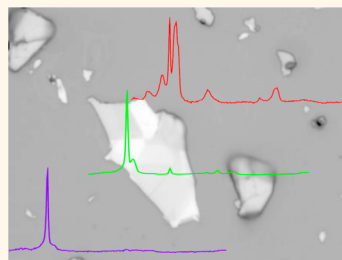
Elena del Corro,*,†,‖ Humberto Terrones,‡ Ana Elias,§ Cristiano Fantini,† Simin Feng,§ Minh An Nguyen,⊥ Thomas E. Mallouk,⊥ Mauricio Terrones,§ and Marcos A. Pimenta†

†Departamento de Fisica, Universidade Federal de Minas Gerais, Av. Antonio Carlos, 6627 Caixa Postal 702 - cep 30, 123-970 Belo Horizonte, MG, Brazil, ‡Department of Physics, Applied Physics and Astronomy, Rensselaer Polytechnic Institute, 110 Eighth Street, Troy, New York 12180, United States, and §Department of Physics and Center for 2-D and Layered Materials and ⊥Department of Chemistry, The Pennsylvania State University, 104 Davey Laboratory, University Park, Pennsylvania 16802, United States. ‖Present address: Electrochemistry Department, J. Heyrovsky Institute of Physical Chemistry of the Academy of Sciences of the Czech Republic, 182 23 Prague, Czech Republic.

ABSTRACT Resonant Raman spectroscopy (RRS) is a very useful tool to study physical properties of materials since it provides information about excitons and their coupling with phonons. We present in this work a RRS study of samples of WSe$_2$ with one, two, and three layers (1L, 2L, and 3L), as well as bulk 2H-WSe$_2$, using up to 20 different laser lines covering the visible range. The first- and second-order Raman features exhibit different resonant behavior, in agreement with the double (and triple) resonance mechanism(s). From the laser energy dependence of the Raman intensities (Raman excitation profile, or REP), we obtained the energies of the excited excitonic states and their dependence with the number of atomic layers. Our results show that Raman enhancement is much stronger for the excited A′ and B′ states, and this result is ascribed to the different exciton—phonon coupling with fundamental and excited excitonic states.

I n recent years, a new family of graphene-like layered inorganic structures has appeared into the scientific scene, and the transition-metal dichalcogenides (TMDs) are now produced as atomically thin structures. Serious efforts are now focused on studying their unique electronic structure, in comparison with their bulk phases.[1−3] Monolayered TMDs, where the metal atom belongs to the sixth column of the periodic table, exhibit a direct gap that evolves to an indirect gap as the number of layers increase.[4] Such an intriguing behavior, and the possibility of producing heterostacked samples including different bidimensional (2D) materials, such as graphene and BN, makes TMDs outstanding candidates for optoelectronic applications. The electronic structure and optical properties of various bulk TMDs were already studied in the past.[5,6] Concerning the electronic and optical properties of monolayered TMD crystals, MoS$_2$ was the first to be investigated,[1,4,7,8] followed by WS$_2$.[2,3,9] However, there exist only few optical studies on WSe$_2$,[3] and most

of them deal with the bulk phase. Here we present a careful investigation of 1L, 2L, 3L, and bulk WSe$_2$ using resonant Raman spectroscopy (RRS), and we were able to obtain not only the excitonic transitions as a function of the number of layers, but also information about electron—phonon coupling in these fascinating systems.

The electronic structure of bulk WSe$_2$ was first calculated by Bromley et al. in 1971,[5] using the semiempirical tight binding method, in a two-dimensional approximation. The optical transmission spectra of bulk WSe$_2$ was measured by Beal et al. in 1972,[6] and compared with the spectra of MoS$_2$ and WS$_2$. These three compounds exhibit two characteristic peaks in the optical absorption spectra in the near-IR and visible region that are ascribed to the so-called A and B excitons. This pair is associated with the lowest energy optical transitions between the spin—orbit split valence band and the lowest conduction band at K and K′ points of the Brillouin zone. For WSe$_2$, the optical absorption spectrum also exhibits a further

* Address correspondence to edelcorro@quim.ucm.es.

doublet (A′, B′) at higher energies. This extra doublet was first ascribed to an interlayer effect, caused by the overlap between anion orbitals of different layers.[6] However, the (A′, B′) doublet was recently observed in the optical spectrum of monolayered WSe₂, showing that its origin can not only be related to an interlayer effect.[3,6] In a recent GW−Bethe−Salpeter first-principles calculation of the optical response of monolayered MoS₂, Qiu et al.[8] predicted the existence of an extra pair of peaks, named as A′ and B′, which are also spin−orbit split states of excitons localized near the K and K′ valleys in the momentum space and correspond to excited states of the exciton pair (A, B). It was also proposed in this work that the lack of the observation of A′ and B′ peaks in the MoS₂ optical spectrum could be due to the short lifetime of the quasiparticles, which broadens the spectrum from the visible to the ultraviolet range.

Raman spectroscopy has turned into a powerful technique for characterizing mainly semiconducting TDMs. The Raman spectrum of various bulk TDMs was measured years ago,[10−13] and the first-order spectrum is dominated by two normal modes with A_{1g} and E_{2g}^1 symmetries. In the particular case of WSe₂, these two modes have practically the same frequency. Additional second-order features, associated with combination and overtones of phonons, also appear in the Raman spectra of TMDs. In this context, Sekine at al. studied the Raman spectra of bulk 2H-MoS₂ using different laser lines and showed that the intensities of both the first- and second-order features are strongly dependent on the laser energy.[14] Stacy and Hodul studied the Raman spectra of bulk 2H-MoS₂ and 2H-WS₂ using different laser lines with energies near the optical absorption edges and demonstrated that the second-order Raman features become stronger as the laser energy approaches the band gap energy.[15] The recent emergence of 2D TMD materials now allows us to investigate the Raman spectra of samples with one, two, or few layers,[16] and it has been noticed that the Raman spectra are significantly dependent on the number of layers.[17,18]

In all previous Raman studies in 2D TMDs,[1,19,20] results were reported with only a few laser excitation lines,[21] thus preventing the determination of the excitation profile (REP) of the Raman features and the dependence on the number of atomic layers. In this work, we present a complete RRS study of 1L, 2L, 3L, and bulk WSe₂ using up to 20 excitation energies in the visible range. We measured the REP of the most intense Raman features, which allowed us to distinguish the behavior of the first- and second-order Raman bands. From the position of the maxima of the REP, it is possible to obtain the energy of the (A′, B′) exciton pair as a function of the number of atomic layers. Our results are in excellent agreement with previous absorption and photoluminescence studies[3] and provide
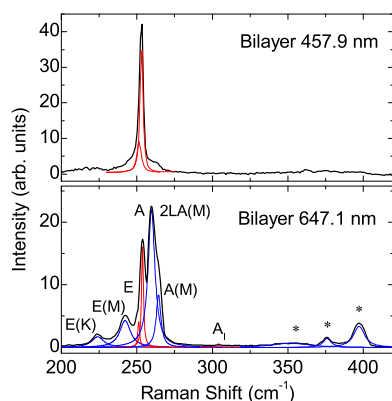

Figure 1. Raman spectrum of bilayer WSe₂ measured with the 457.9 and 647.1 nm excitation wavelengths in the spectral range from 200 to 450 cm⁻¹. Red and blue lines represent the Lorentzian fitting functions of first- and second-order bands, respectively. *See the assignment in Table 1.

experimental support for the interpretation of the (A′, B′) pair in the spectrum of WSe₂. Our study also provides new information about exciton−phonon interactions in 2D WSe₂ with different number of layers and shows the suitability of RRS as a nondestructive tool for addressing the structural dependence of the electronic properties in 2D semiconducting TMDs.

RESULTS

First- and Second-Order Raman Spectrum. The Raman spectra of 2D WSe₂ crystals with different number of layers have been recently described.[17,18] Although bulk 2H-TMDs belong to the D_{6h} point group, odd and even few layer TMDs belong to the D_{3h} and D_{3d} point groups, respectively. Therefore, the Raman modes with A_{1g} and E_{2g} symmetries for bulk TMDs become modes with A_1' and E' symmetry for odd few layers TMDs and modes with A_{1g} and E_g for even few layers TMDs. In this work, and for simplicity, we decided to label these modes just as A and E for all our samples.

As an example, in Figure 1 we present Raman spectra of bilayer WSe₂ sample measured with the 457.9 and 647.1 nm laser lines (2.54 and 1.92 eV laser energies, respectively) in the 200 to 450 cm⁻¹ spectral range. In the 457.9 nm spectrum, one can observe a single peak associated with the two first-order Raman modes with A and E symmetries, which have practically the same frequency, appearing at around 249 and 251 cm⁻¹, respectively. This accidental degeneracy prevents a clear identification of the two contributions in the spectrum. The evolution of these two first-order modes with the number of layers has been recently described using three different excitation energies, considering polarized Raman experiments, and it was shown that the frequency shift between the two bands can be used to determine the number of layers in the sample.[21]

In the 647.1 nm spectrum, it is possible to observe a number of features, below and above the first-order

peak (A + E) around 250 cm^{-1}, that are associated with second-order processes involving two phonons within the interior of the Brillouin zone or involving one phonon and a defect. The two features located at 260 and 263 cm^{-1} might correspond, respectively, to the overtone of the LA phonon branch at the M point (named as the 2LA(M) feature) and to a phonon belonging to the A-symmetry optic branch at the M point, which becomes active due to structural disorder, similar to the disorder-induced D band in graphene[22] (labeled A(M) in this work). Further contributions, not described before in the literature, appear around 225 and 242 cm^{-1}. On the basis of our theoretical predictions, these contributions might correspond to a phonon mode of the E-symmetry optic branch at the K and M points of the Brillouin zone, respectively, that are also activated by disorder (we will refer to them as E(K) and E(M)). We can also observe other weak contributions in the spectral range from 300 to 400 cm^{-1}. The first one appears at ca. 305 cm^{-1}, and its origin has been recently reported as an A-symmetry first-order mode corresponding to an interlayer vibration, which becomes a Raman active mode for samples consisting of just a few layers, bi and trilayer in our case;[17,18] we will refer to this feature as the A_I band (I standing for interlayer). At slightly higher frequencies, we can observe a group of three peaks around 360, 375, and 395 cm^{-1}. A preliminary assignment of these bands can be found in ref 21, and in Table 1 we present a more detailed assignment combined from ref 21 and our theoretical calculations. The origin of all these second-order features is not yet well established; in contrast with the assignment presented here, a recent publication proposes the participation of the transversal acoustic modes in the existence of these resonant bands.[23]

Resonance Raman Results. As shown in Figure 1, the Raman spectra of 2D WSe$_2$ crystals are strongly dependent on the laser line used to collect the data. In order to address this issue, all samples in this work were investigated with 20 different laser lines in a wide range of excitation energies. In Figure 2, we display selected resonant Raman spectra of WSe$_2$ samples with one to three layers, as well as the bulk, collected with different laser lines. Despite the fact that the relative intensities of all Raman features are strongly dependent on the laser excitation as well as on the number of atomic layers, the decomposition of the registered spectra as a sum of individual peaks reveals that none of the described peaks shifts with the excitation energy. This is an expected result for the first-order modes, but in the case of the second-order bands, it indicates that these bands involve phonons within the interior of the Brillouin zone belonging to almost nondispersive branches (similarly to the LA phonon dispersion curve close to the M point).

All recorded spectra were fit as a sum of Lorentzian curves, allowing us to obtain the REPs of all Raman

TABLE 1. Assignment of the Second-Order Raman Contributions in the Spectral Range from 200 to 400 cm^{-1}

band (cm^{-1})	assignment[a]
225	E(K)[a]
242	E(M)[a]
260	2LA(M)[a,b]
263	A(M)[a]
360	$2E_{1g}(\Gamma)$[b] or $A_{1g}(M) + TA(M)$[b]; $2E'(\Gamma) - LA(K)$[a] and $2A'_1(\Gamma) - LA(K)$[a]
375	$E^1_{2g}(M) + LA(M)$[b], $E'(\Gamma) + LA(M)$[a], and $A'_1(\Gamma) + LA(M)$[a]
395	$E'(\Gamma) + LA(K)$[a] and $A'_1(\Gamma) + LA(K)$[a] and $3LA(M)$[a,b]

[a] The a and b superscripts stand for this work and ref 21, respectively.

bands, that is, Raman intensity *vs* laser excitation energy. The intensities were normalized according to the intensity of the silicon peak, taking into account the Si Raman cross-section at each excitation energy, reported in ref 24. We analyzed the combined intensity of the first-order band around 250 cm^{-1}, associated with both the E + A modes, as a function of the excitation energy, since the two individual peaks are almost degenerated, thus preventing a clear distinction of the contribution of each one to the total enhancement. The same procedure was used to analyze the band around 260 cm^{-1}, associated with both second-order processes 2LA(M) and A(M). In this way, we were able to accurately distinguish between the behavior of the REP for the first- and second-order bands.

Parts A and B of Figure 3 show, respectively, the REP of the first-order band around 250 cm^{-1} and the second-order band around 260 cm^{-1} for all the samples studied in this work. We can first observe that the REPs of the first- and second-order features are different. For monolayer WSe$_2$, the REP of the first-order peaks exhibit only one large maximum around 2.4 eV, whereas the REP of the second-order bands, also exhibit a second maximum at lower energies, around 2.1 eV. The energy separation of these two maxima for the second-order features decreases when we add more layers, and they converge to a single maximum for bulk WSe$_2$. We can also observe in the REP of the first-order features the existence of another weak maximum in the range 2.5−2.8 eV, which will be discussed in the next section. Using the same procedure discussed above, it is possible to obtain the Raman excitation profile of all other Raman features, and the complete analysis of our results is shown in the Supporting Information. We have observed that the REPs of all second-order Raman features are similar to those shown in Figure 3B.

DISCUSSION

As explained above, the Raman signal can be enhanced when either the incident or scattered photons are in resonance with electronic (or excitonic) transitions.
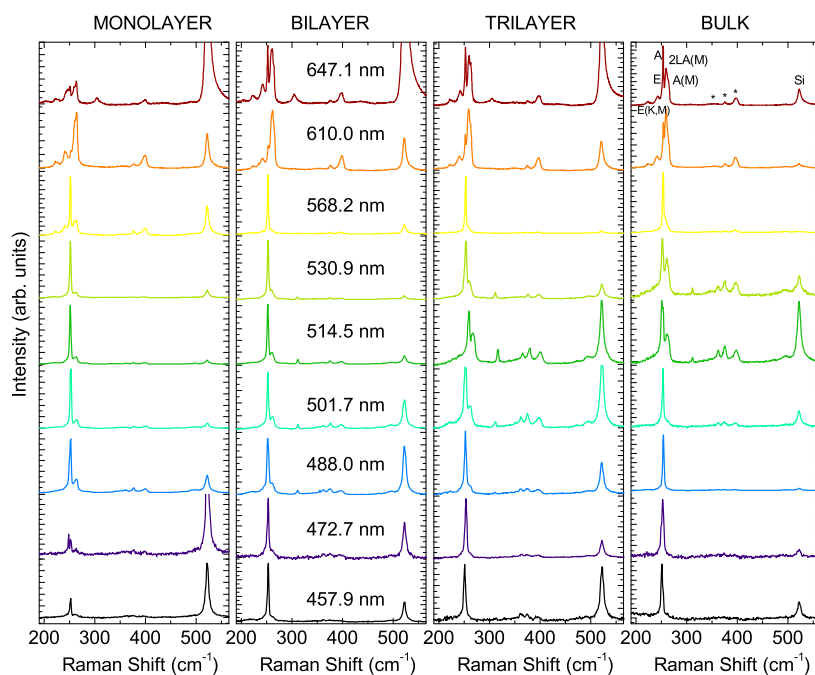
Figure 2. Selected Raman spectra of WSe$_2$ samples with different number of layers registered with a wide range of excitation wavelengths. The peak at 520 cm^{-1} comes from the silicon substrate and was used for intensity normalization.
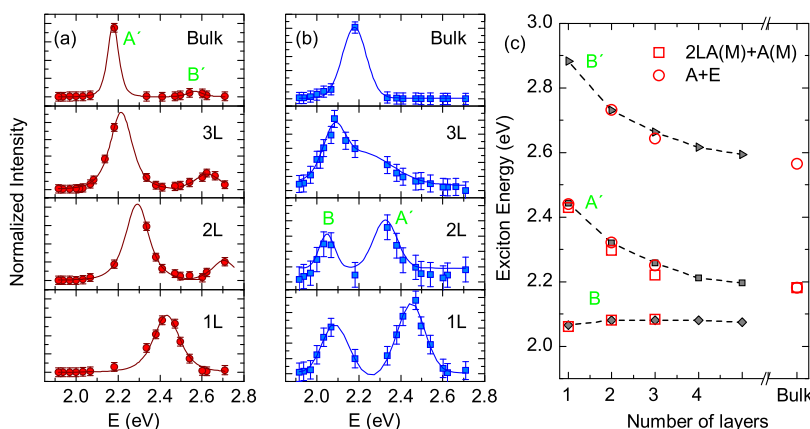

Figure 3. Evolution of the REP with the number of layers for (a) the first-order modes (A + E) and (b) the second-order bands (2LA(M) + A(M)). The first-order modes (in red) are fitted according to eq 1, whereas the second-order bands (in blue) are fitted with Gaussian functions. (c) Comparison between the position of the Raman signal enhancement obtained in this work (open symbols) and the absorption data derived from ref 3 (solid symbols).

For a first-order Raman process, the intensity of a Raman peaks as a function of the laser energy can be described by the Fermi golden rule for a third-order time dependent perturbation theory process, given by

$$I(E \text{ laser}) = C \left| \sum_{a,b} \frac{\langle f|H_{e-r}|b\rangle\langle b|H_{e-ph}|a\rangle\langle a|H_{e-r}|i\rangle}{(E_{laser} - E_{gap} - i\gamma)(E_{laser} - E_{gap} + E_{ph} - i\gamma)} \right|^2 \quad (1)$$

where γ is the damping factor accounting for the inverse lifetime of the excited electronic state in the resonant scattering process,[25] and the phonon energy E_{ph} is fixed to the frequency of the analyzed Raman feature. The two terms in the denominator of eq 1

give rise to the enhancement of the first-order Raman feature when the incident or scattered photons are in resonance with electronic (or excitonic) transitions. The three terms in the numerator correspond to the matrix elements for the electron−photon Hamiltonian (emission of the scattered photon), electron−phonon Hamiltonian (creation of one phonon), and electron−photon Hamiltonian (absorption of the incident photon), respectively. The difference between considering interactions of photons and phonons with electrons or excitons is provided by the quantum states and not by the perturbation Hamiltonians, which are the same for both electrons and excitons.[26] Therefore, eq 1 is valid for both cases.

As already mentioned, the optical absorption spectra of WSe_2 exhibit four peaks in the near IR and visible region that are ascribed to the two pairs of excitons, (A, B) and (A′, B′). For monolayered WSe_2, these four peaks appear, respectively, at 1.65, 2.05, 2.40, and 2.80 eV. An important result shown in Figure 3A is the fact that the first-order (A+E) Raman features are not enhanced (or very weakly enhanced) using laser energies corresponding to the B exciton (the A exciton is out of the range of laser energies used in this work). Interestingly, the REP of this first-order band exhibits a strong enhancement for laser energies near the A′ and B′ exciton energies (the resonance with exciton B′ is not observed for monolayer WSe_2 due to the excitation range covered in our experiments). This result can be understood by considering the middle term in the numerator of eq 1, which gives the strength of the electron−phonon coupling. It reveals that the coupling of these first-order phonons is stronger for the (A′, B′) pair, showing that RRS provides information about electron−phonon coupling in TMDs, which cannot be obtained in optical absorption and photoluminescence experiments. Figure 3A also shows the fitting of the experimental first-order REP data by eq 1, and the fitting parameters are summarized in Table 2. From these data we can observe the evolution of the splitting (B′−A′) with the number of layers. Such energy difference can be associated with both the spin−orbit coupling (SOC)[27] and the interlayer interaction; however the precision of our experimental data prevent us from discerning between both effects, since the difference (B′−A′) remain constant in about (0.40 ± 0.02) eV for the three samples.

Second-order Raman features involve, in general, two phonon modes within the interior of the Brillouin zone, and their intensities are described by a fourth-order time dependent perturbation theory expression. Therefore, eq 1 is not adequate to fit the REP of these second-order features. Since the precise assignment of these second-order features is not yet completely established, Gaussian functions have been used to fit the REPs shown in Figure 3B and to determine the Raman enhancement energies. Contrary to the case of the first-order features, which are only enhanced at laser energies corresponding to the A′ and B′ excitons, the second-order Raman bands exhibit a quite different Raman excitation profile behavior: we can also observe in Figure 3B a maximum at a lower energy, in a position that coincides with that of the B exciton. The different behavior of the REPs of the first- and second-order features is, in fact, an expected result. First, for a second-order process, there are three terms in the denominator of the Fermi golden rule expression,[28] and therefore, the resonance conditions are different from those described by the first-order expression given in eq 1. Moreover, the phonons involved in the second-order process are not at the Γ point of the

TABLE 2. Fitting Parameters, in eV, of the Full Curves Shown in Figure 3A

	A′		B′	
	E_{gap}	γ	E_{gap}	γ
1L	2.42	0.22		
2L	2.28	0.20	2.69	0.20
3L	2.20	0.19	2.61	0.22
bulk	2.16	0.08	2.55	0.13

Brillouin zone, and their symmetries depend on their specific wavevector (q value). Consequently, the electron−phonon matrix elements involved in a second-order process are not the same than those of the first-order modes that take place at the center of the Brillouin zone. The fact that the second-order Raman features can be more intense than the first-order peaks for laser energies in resonance with exciton B supports the double-resonance mechanism for the enhancement of these bands, similarly to what occurs in graphene systems.[22,28]

Let us finally discuss the dependence of the maxima in the REPs with the number of layers and compare them with previous results of optical studies in WSe_2. Figure 3C shows how the B, A′, and B′ exciton energies, obtained from optical absorption,[3] vary with the number of layers. It was also shown in ref 3 that the energies of the A and B peaks are weakly dependent on the flake thickness, whereas the energies of the A′ and B′ peaks blueshift with decreasing the thickness of the WSe_2 samples. We also plot in Figure 3C the energies obtained from our Raman results. We observe that there is an excellent agreement between the resonant Raman and optical data and their dependence with the number of layers. While the pair (A′, B′) energy decreases with the number of layers, the B exciton energy slightly increases with increasing number of layers. This is reason why, in bulk samples, only a single enhancement is observed around 2.20 eV, associated with both the B and A′ excitons.

CONCLUSIONS

In summary, we have investigated in this work the resonant Raman spectra of WSe_2 samples with one, two, and three atomic layers (1L, 2L, 3L) and bulk WSe_2, using 20 different laser lines in the visible range. We were able to obtain the Raman excitation profile of the first- and second-order Raman features, which exhibit different behaviors, and shows that the second-order features come from a double (and triple) resonance mechanism(s). From these REPs, we have obtained the energies of the excited excitonic states and their dependence with the number of atomic layers, which are in excellent agreement with previous optical studies. Moreover, we observed that the enhancement of the first-order Raman modes are much stronger for
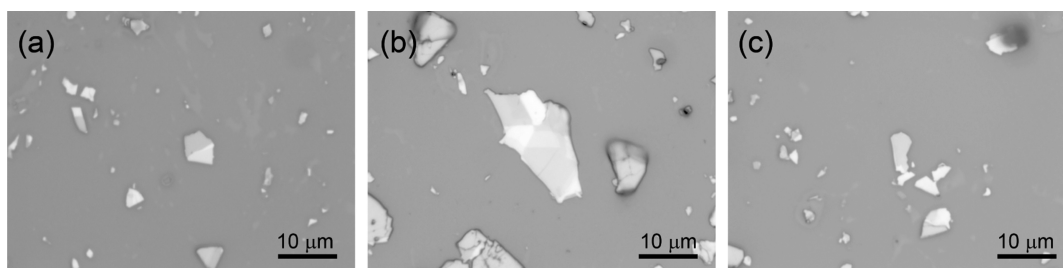
Figure 4. Photographs of the measured WSe₂ flakes with (a) one, (b) two, and (c) three layers and the bulk.

resonances with the (A′, B′) excited excitonic pair than with the (A, B) fundamental pair. Since Raman scattering involves both electron−photon and electron−phonon interactions (in contrast with optical absorption that only involves the electron-photon one), this result indicates that the electron−phonon coupling is different for the ground and the excited exciton states.

METHODS

Bulk 2H-WSe₂ crystals were produced using the chemical vapor transport method described elsewhere.[16] The crystals were mechanically exfoliated and deposited on Si/SiO₂ substrates to obtain the few-layered samples. In Figure 4 we present photographs of the studied flakes, which present dimensions larger than 20 μm². The Raman spectra were registered in backscattering geometry using a triple monochromator spectrometer DILOR XY with different laser sources (Ar/Kr and a dye laser with Rhodamine 6G and DCM-special dyes) to excite the sample using 20 different laser lines in a wide energy range from 457.9 to 650.0 nm. The laser power was kept below 0.6 mW to avoid damage of the sample. The samples were focused by a 100× (N.A. 0.95) objective. Accumulation times between 1 and 20 min were needed depending on the excitation energy and the number of layers in the sample.

Conflict of Interest: The authors declare no competing financial interest.

Supporting Information Available: Raman excitation profile of the less intense contribution in the Raman spectrum of WSe₂. This material is available free of charge *via* the Internet at http://pubs.acs.org

REFERENCES AND NOTES

1. Tonndorf, P.; Schmidt, R.; Böttger, P.; Zhang, X.; Börner, J.; Liebig, A.; Albrecht, M.; Kloc, C.; Gordan, O.; Dietrich, R.; *et al.* Photoluminescence Emission And Raman Response of Monolayer MoS₂, MoSe₂, and WSe₂. *Opt. Express* **2013**, *21*, 4908–4916.
2. Kuc, A.; Zibouche, N.; Heine, T. Influence of Quantum Confinement on the Electronic Structure of the Transition Metal Sulfide TS₂. *Phys. Rev. B* **2011**, *83*, 245213.
3. Zhao, W.; Ghorannevis, Z.; Chu, L.; Toh, M.; Kloc, C.; Tan, P.-H.; Eda, G. Evolution of Electronic Structure in Atomically Thin Sheets of WS₂ and WSe₂. *ACS Nano* **2013**, *7*, 791–797.
4. Mak, K. F.; Lee, C.; Hone, J.; Shan, J.; Heinz, T. F. Atomically Thin MoS₂: A New Direct-Gap Semiconductor. *Phys. Rev. Lett.* **2010**, *105*, 136805.
5. Bromley, R. A.; Murray, R. B.; Yofee, A. D. The Band Structures of Some Transition Metal Dichalcogenides: III. Group VI A: Trigonal Prism Materials. *J. Phys. C: Solid State Phys.* **1972**, *5*, 759–778.
6. Beal, A. R.; Knights, J. C.; Liang, W. Y. Transmission Spectra of Some Transition Metal Dichalcogenides: II. Group VIA: Trigonal Prismatic Coordination. *J. Phys. C: Solid State Phys.* **1972**, *5*, 3540–3551.
7. Fan, J-He.; Gao, P.; Zhang, A.-M.; Zhu, B.-R.; Zeng, H.-L.; Cui, X.-D.; He, R.; Zhang, Q.-M. Resonance Raman Scattering in Bulk 2H-MX₂ (M = Mo, W; X = S, Se) and Monolayer MoS₂. *J. Appl. Phys.* **2014**, *115*, 053527.
8. Qiu, D. Y.; da Jornada, F. H.; Louie, S. G. Optical Spectrum of MoS₂: Many-Body Effects and Diversity of Exciton States. *Phys. Rev. Lett.* **2013**, *111*, 216805.
9. Gutierrez, H. R.; Perea-Lopez, N.; Elías, A. L.; Berkdemir, A.; Wang, B.; Lv, R.; Lopez-Urías, F.; Crespi, V. H.; Terrones, H.; Terrones, M. Extraordinary Room-Temperature Photoluminescence in Triangular WS₂ Monolayers. *Nano Lett.* **2013**, *13*, 3447–3454.
10. Sekine, T.; Izumi, M.; Nakashizu, T.; Uchinokura, K.; Matsuura, E. Raman Scattering And Infrared Reflectance in 2H-MoSe₂. *J. Phys. Soc. Jpn.* **1980**, *49*, 1069–1077.
11. Chen, J. M.; Wang, C. S. Second Order Raman Spectrum of MoS₂. *Solid State Commun.* **1974**, *14*, 857–860.
12. Sekine, T.; Nakashizu, T.; Toyoda, K.; Uchinokura, K.; Matsuura, E. Raman Scattering in Layered Compound 2H-WS₂. *Solid State Commun.* **1980**, *35*, 371–373.
13. Sourisseau, C.; Cruege, F.; Fouassier, M.; Alba, M. Second-Order Raman Effects, Inelastic Neutron Scattering And Lattice Dynamics in 2H-WS₂. *Chem. Phys.* **1991**, *150*, 281–293.
14. Sekine, T.; Uchinokura, K.; Nakashizu, T.; Matsuura, E. Dispersive Raman Mode of Layered Compound 2H-MoSe₂ Under Resonant Condition. *J. Phys. Soc. Jpn.* **1984**, *53*, 811–818.
15. Stacy, A. M.; Hodul, D. T. Raman Spectra of IVB And VIB Transition Metal Disulfides Using Laser Energies Near the Absorption Edges. *J. Phys. Chem. Solids* **1985**, *46*, 405409.
16. Berkdemir, A.; Gutierrez, H. R.; Botello-Mendez, A. R.; Perea-Lopez, N.; Elias, A. L.; Chia, C.-I.; Wang, B.; Crespi, V. H.; Lopez-Urias, F.; Charlier, J.-C.; *et al.* Identification of Individual And Few Layers of WS₂ Using Raman Spectroscopy. *Sci. Rep.* **2013**, *3*, 1755.
17. Luo, X.; Zhao, Y.; Zhang, J.; Toh, M.; Kloc, C.; Xiong, Q.; Quek, S. Y. Effects of Lower Symmetry And Dimensionality on Raman Spectra in 2D WSe₂. *Phys. Rev. B* **2013**, *88*, 195313.
18. Terrones, H.; Del Corro-Garcia, E.; Feng, S.; Poumirol, J. M.; Rhodes, D.; Smirnov, D.; Pradhan, N. R.; Lin, Z.; Nguyen, M. A. T.; Elias, A. L.; *et al.* New First Order Raman-Active Modes in Few Layered Transition Metal Dichalcogenides. *Sci. Rep.* **2014**, *4*, 4215.

19. Najmaei, S.; Liu, Z.; Ajayan, P. M.; Lou, J. Thermal Effects on the Characteristic Raman Spectrum of Molybdenum Disulfide (MoS$_2$) of Varying Thicknesses. *Appl. Phys. Lett.* **2012**, *100*, 013106.

20. Chakraborty, B.; Ramakrishna-Matte, H. S. S.; Sood, A. K.; Rao, C. N. R. Layer-Dependent Resonant Raman Scattering of a Few Layer MoS$_2$. *J. Raman Spectrosc.* **2013**, *44*, 92–96.

21. Zhao, W.; Ghorannevis, Z.; Kumar, A. K.; Pang, J. R.; Toh, M.; Zhang, X.; Kloc, C.; Tan, P. H.; Eda, G. Lattice Dynamics in Mono- and Few-Layer Sheets of WS$_2$ and WSe$_2$. *Nanoscale* **2013**, *5*, 9677.

22. Pimenta, M. A.; Dresselhaus, G.; Dresselhaus, M. S.; Cançado, L. G.; Jorio, A.; Saito, R. Studying Disorder in Graphite-Based Systems by Raman Spectroscopy. *Phys. Chem. Chem. Phys.* **2007**, *9*, 1276–91.

23. Goasa, K.; Grzeszczyk, M.; Leszczyski, P.; Faugeras, C.; Nicolet, A. A. L.; Wysmoek, A.; Potemski, M.; Babiski, A. Multiphonon Resonant Raman Scattering in MoS$_2$. *Appl. Phys. Lett.* **2014**, *104*, 092106.

24. Lautenschlager, P.; Garriga, M.; Vina, L.; Cardona, M. Temperature Dependence of the Dielectric Function and Interband Critical Points in Silicon. *Phys. Rev. B* **1987**, *36*, 4821.

25. Jorio, A.; Souza Filho, A. G.; Dresselhaus, G.; Dresselhaus, M. S.; Saito, R.; Hafner, J. H.; Lieber, C. M.; Matinaga, F. M.; Dantas, M. S. S.; Pimenta, M. A. Joint Density of Electronic States for One Isolated Single-Wall Carbon Nanotube Studied by Resonant Raman Scattering. *Phys. Rev. B* **2001**, *63*, 245416.

26. Yu, P. Y.; Cardona, M. *Fundamentals of Semiconductors, Physics and Materials Properties*, 3rd ed.; Springer: Berlin, 2005.

27. Sun, L.; Yan, J.; Zhan, D.; Liu, L.; Hu, H.; Li, H.; Tay, B. K.; Kuo, J.-L.; Huang, C.-C.; Hewak, D. W.; *et al.* Spin-Orbit Splitting in Single-Layer MoS$_2$ Revealed by Triply Resonant Raman Scattering. *Phys. Rev. Lett.* **2013**, *111*, 126801.

28. Venezuela, P.; Lazzeri, M.; Mauri, F. Theory of Double-Resonant Raman Spectra in Graphene: Intensity and Line Shape of Defect-Induced And Two-Phonon Bands. *Phys. Rev. B* **2011**, *84*, 035433.